Journal of Power Sources 218 (2012) 405–411

Contents lists available at SciVerse ScienceDirect

Journal of Power Sources

journal homepage: www.elsevier.com/locate/jpowsour

Nanograss-structured counter electrode for dye-sensitized solar cells

Wei Jiang [1], Lei Yin [1], Hongzhong Liu*, Yucheng Ding

State Key Laboratory for Manufacturing Systems Engineering, Xi'an Jiaotong University, Xi'an 710049, China

HIGHLIGHTS

- Exploring the method of structuring the counter electrode.
- A simple one-step approach to the maskless fabrication of nanograss structure.
- Structured counter electrode evidently reduces the charge-transfer resistance.
- Structured counter electrode largely improves the light absorption.

ARTICLE INFO

Article history:
Received 12 April 2012
Received in revised form
4 June 2012
Accepted 7 June 2012
Available online 2 July 2012

Keywords:
Solar cells
Silicon nanograss
Counter electrode
Charge-transfer resistance

ABSTRACT

In order to improve the electrochemical and optical performance of counter electrode for solar cells, a nanograss-structured electrode on silicon is explored as counter electrode for dye-sensitized solar cells (DSSCs). The nanograss-structured counter electrode is fabricated by dry etching of silicon and followed by metal deposition. The morphological, electrochemical and optical properties of the counter electrode are characterized by scanning electron microscopy, electrochemical impedance spectroscopy and reflection spectroscopy, respectively. Compared with traditional planar counter electrodes, the energy-conversion efficiency, fill factor and short-circuit current are increased by 15.1%, 1.5% and 12.1% by the nanograss-structured counter electrode for DSSCs, respectively. The results also show that, the nanograss-structured counter electrode can effectively enhance the light scattering, provide a larger contact area with electrolyte/Pt, and reduce the charge-transfer resistance.

1. Introduction

Dye-sensitized solar cells (DSSCs), composed of nanocrystalline semiconductor, sensitizer, electrolyte, and platinized counter electrode, have attracted much attention of the researchers. In recent years, the efficiency of the DSSCs has reached up to 12% under simulated solar light (AM1.5) [1], rendering it credible to be one of the most promising candidates compared to conventional silicon-based solar cells [2].

In the development of DSSCs, the counter electrode is an important component, which acts as a role to transfer the electrons from external circuit back to the electrolyte and catalyzing the reduction of triiodide; moreover, the light reflection and scattering by the counter electrode can increase light absorption of the photo-anode. Therefore, the counter electrode, with high electrochemical activity and excellent optical characteristics, is desirable to an efficient dye-sensitized solar cell [3].

Currently, counter electrodes have been under widely investigated, however, most research is focused on developing new substitution material investigations or different platinum coating processes. For the developed substitution materials acting as counter electrodes for DSSCs, such as carbon black [4], carbon nanotubes [5], graphite [6–8] and various polymers [9,10], they all exhibit excellent catalytic properties comparable with that of platinum. Among these materials, DSSCs made with platinum currently show much higher energy-conversion efficiencies [11], because of their excellent electro-catalytic performance, chemical and thermal stability, and strong light reflection [12]. For the new platinum coating processes to fabricate counter electrodes for dye-sensitized solar cells, such as electrochemical deposition and thermal treatment [13], electrochemical reduction, electron-beam evaporation, sputtering [14], thermal decomposition of H_2PtCl_6 [15–17], and self-assembly of Pt nanoparticles [18], the performances were similar to each other, because the platinum particles produced by the different methods mentioned above have similar catalytic activity and zerovalent.

So, new methods to improve the performance of counter electrode are still being developed. A structure-engineered counter

* Corresponding author. Tel.: +86 29 83395021; fax: +86 29 83399512.
E-mail address: hzliu@mail.xjtu.edu.cn (H. Liu).
[1] These authors contributed equally to this work.

0378-7753/$ – see front matter © 2012 Elsevier B.V. All rights reserved.
http://dx.doi.org/10.1016/j.jpowsour.2012.06.033

electrode is one of the potential ways to enhance the light absorption and thus improve the performance of DSSCs. To the best of our knowledge, however, little attention has been paid to the effect of structure-engineered counter electrodes. In this paper, we develop an innovative nanograss-structured counter electrode for dye-sensitized solar cells (DSSCs), which has a significant improvement in the electrochemical active surface of electrodes and light absorption. The nanograss-structured counter electrode was fabricated by dry etching of silicon followed by metal deposition [19–21]. This process is simple and low-cost, moreover, it is compatible with large area fabrication processes of DSSCs [22]. Fig. 1 shows the schematic diagram of the DSSCs with nanaograss-structured counter electrode in this study.

In this paper, effects of the nanograss-structured counter electrode on wetting characteristics for electrolyte, current–voltage curves, electrochemical impedance spectroscopy, reflection spectroscopy and other performance parameters of the cells were evaluated and discussed. We found that the structured counter electrode with enlarged surface area, enhanced catalysis efficiency and improved light scattering, may be a preferred choice for improving the performance of the DSSCs. Compared with the traditional planar counter electrode, the energy-conversion efficiency, fill factor and short-circuit current were improved by 15.1% 1.5% and 12.1%, respectively.

2. Experimental details

2.1. Fabrication and characterization of nanograss structure on silicon

Nanograss structure has been obtained by various techniques, such as optical lithography, electron-beam lithography, and etching with porous anodic alumina, nanoparticles or nanospheres as masks [23,24]. In this paper, inductive-coupled reactive (ICP) ion etching process was employed to produce perfectly aligned, and free standing nanograss structure on silicon, and the height and diameter of the nanograss structure were precisely controlled. The ICP etching process for silicon nanograss is based on the appropriate Boss process parameters of ICP, which employs alternate cycles of etching and passivation. Sulfur hexafluoride (SF_6) was used for etching, and octafluorocyclobutane (C_4F_8) for passivation. The Boss process parameters with SF_6 were at 70–150 sccm for 7–15 s and C_4F_8 at 100–200 sccm for 10–20 s. The RF power at 600–800 W was used for various silicon nanograss growths. A longer time of Boss process resulted in longer nanograss, but further increasing time can result in self-contraction of nanograss in length. The length of the nanograss can reach to roughly 200 nm to 20 μm long. The ratio of SF_6/C_4F_8 determines the diameters and the density of the nanograss. After preparing silicon nanograss, magnetron-sputtering process was employed to deposit platinum nanoparticles on the prepared silicon nanosgrass, which in order to better serve as the counter electrodes compared to other catalyst materials.

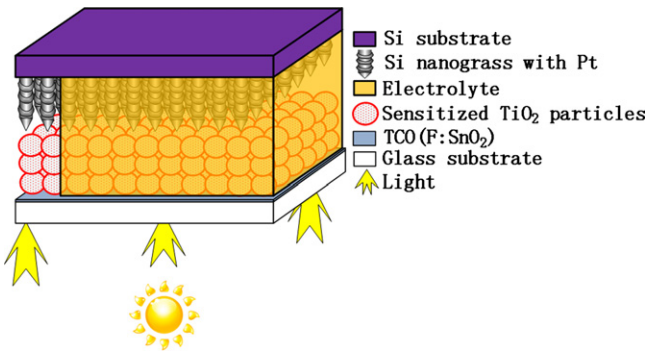

Fig. 1. Schematic diagram of the preliminary structure of DSSCs based on the nanograss-structured counter electrode.

2.2. Fabrication and characterization of DSSCs

To fabricate a DSSC TiO_2 photo-anode, a finely grinded TiO_2 paste, consisting of 3 g TiO_2 (P25 Degussa) powder, 0.1 ml acetylacetone, 0.05 ml Triton X-100 and 15 ml distilled water, was prepared by grinding for 3 h in a mortar. Afterward the grinded TiO_2 paste was coated by doctor blade technique on a FTO-coated glass (Nippon Sheet Glass, ~15 Ω/□, 2.2 mm thick), which is cleaned by ethanol, acetone and distilled water in ultrasonic bath before coating process. After baking at 90 °C for 10 min, the TiO_2 photo-anode was sintered at 450 °C for 30 min and then cooled to 80 °C in ambient condition. Subsequently, the photo-anode was impregnated with a 0.3 mM ethanol solution of N719 dye (dye Ruthenium 535-bisTBA, Solaronix, Switzerland) for at least 12 h at room temperature. The excess unanchored dyes were rinsed off by absolute ethanol and dried in air. The sensitized electrode was sandwiched with platinum-coated nanograss-structured counter electrode separated by a hot-melt spacer (60 μm in thickness, Dupont 1702). A drop of the redox electrolyte, containing 0.1 M LiI, 0.05 M I_2, 0.5 M 4-tertbutylpyridine, and 0.6 M 1,2-dimethyl-3-propylimidazoium in acetonitrile solution, was dipped on the hole in the counter electrode, The active cell area was typically 0.25 cm^2. All the chemicals referred above were purchased and directly used without further purification.

2.3. Measurements

The morphology of the counter electrodes was observed by scanning electron microscopy (SEM). The electrolyte wetting behavior of the nanograss structure was characterized by a contact angle measuring device (OCA 20, DataPhysics). The optical reflection spectra of the counter electrode were examined by a UV–VIS–NIR spectrophotometer (Jasco-V-570). The photocurrent density-voltage (J–V) characteristics were evaluated by a 300 W Xeon light source (calibrated with standard solar cells), AM 1.5G illumination (100 mW cm^{-2} in intensity), and a Keithley digital source meter (Model 2612). Electrochemical impedance spectra (EIS) of the blank cells were evaluated by using CHI-660D at zero bias potential and over the frequency range of 10^{-2}–10^5 Hz with 10 mV AC signal. The blank cells, consisting of two identical counter electrodes and three layers of Scotch Magic Tape (around 120 μm thick) in between as spacer, have an active area about 0.25 cm^2. The EIS measurements of the assembled DSSCs were recorded at the open-circuit voltage of the devices and in the frequency range between 0.05 Hz and 10^6 Hz under an illumination of 100 mW cm^{-2}.

3. Results and discussion

3.1. The surface morphology of the counter electrode

The morphology and structure of the prepared various nanograss-structured Pt counter electrode were observed by means of scanning electron microscope (SEM). Fig. 2 shows the typical SEM images of the prepared nanaograss-structured counter electrode. The morphology of silicon nanograss structure was controlled by the etching processing parameters described in Section 2. Fig. 2a shows the morphology of the submicron silicon nanograss, the Pt layer on the structured surface is elliptical in the

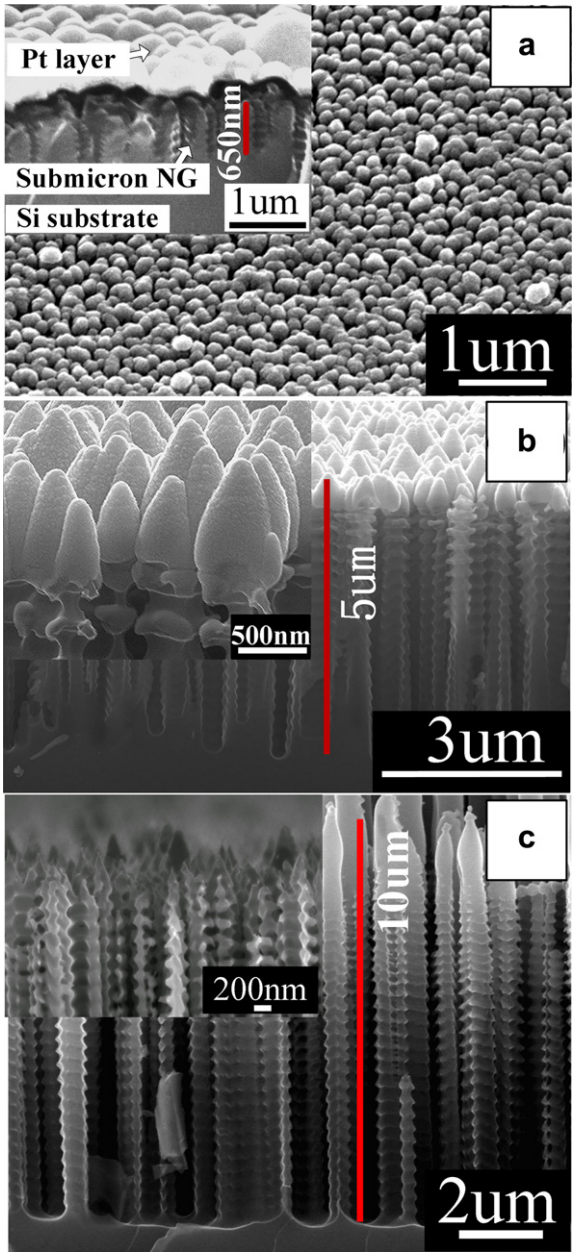

Fig. 2. Well-aligned silicon nanograss arrays on a silicon wafer are shown. (a) The elliptical surface morphology of submicron nanograss structure, the inset shows the magnified image of the cross section. (b) Cross section images of the nanograss arrays with 5 μm length, and the inset shows the magnified image with Pt particles on the top surface of the silicon nanograss. (c) Cross section images of the nanograss arrays with 10 μm length and there are no Pt particles sputtered on the surface of the silicon nanograss, and the inset shows the magnified image of the pure silicon nanograss arrays.

view of the overall morphology. Furthermore, from the inset of Fig. 2a, we can find that Pt layer on the silicon nanograss surface is uniform, compact and continuous. In Fig. 2b, it is evident that Pt layer on the well-aligned silicon nanograss is discontinuous and the inset magnified image presents that only the top of the nanograss was coated with Pt particles. Fig. 2c exhibits that the nanograss arrays with the length about 10 μm are in order, backbone-like morphology along their height. The diameter of the nanograss is about 200–300 nm. Recently, similar incensement of the surface roughness has been revealed in black silicon prepared by reactive ion etching approach, when compared with the conventional planar counter electrode [25,26]. Thus, similarly it can be deduced from the surface morphologies that, the nanograss-structured counter electrode with particularly large surface area and unique ordered nanostructure can decrease the resistances of charge transfer, accelerate the electrolyte diffusion and increase the light absorption, which are determining factors affecting the DSSC performance.

3.2. Wetting characteristics of the nanograss-structured counter electrode

It is clear that the nanograss-structured morphology of counter electrode can supply potential larger contact area between electrolyte and counter electrode than conventional planar morphology. However, whether electrolyte can go into the gaps and form an excellent contact with counter electrode determine the electron transfer and ion movement, thus affecting the final performance of DSSCs. So, it is important to investigate the wettability of the structured counter electrode. Contact angles of water and electrolyte on the structured surfaces (before and after metal deposition, respectively) are examined to indicate the wettability of the structured counter electrode, as shown in Fig. 3. From Fig. 3, it is evident that, before Pt deposition, the nanograss structure with 5 μm in length exhibits excellent repellence with a high contact angle above 160° for water and 110° for electrolyte. After Pt deposition, the contact angle reduces to 130° for water and almost 0° for electrolyte. The nearly 0° contact angle for electrolyte indicates that electrolyte can fill into the gaps on the electrode surface, and form a good contact with the counter electrode. For comparison, the contact angles of water and electrolyte on the planar counter electrode (by Pt deposition on planar silicon) were also measured, and it shows a contact angle of 98° for water and 30° for electrolyte. So, the nanograss-structured counter electrode is much easier to wet with electrolyte than planar electrode, which indicates that the nanograss-structured counter electrode can supply larger contact area and better contact with electrolyte. Therefore, the nanograss-structured counter electrode can be expected to supply an excellent catalytic activity for triiodide reduction.

3.3. Photovoltaic performance

In order to demonstrate the effects of structured counter electrode, four different kinds of counter electrodes, such as planar electrode, submicron-NG electrode, 5 μm NG electrode and 10 μm NG electrode, were prepared, and their effects on DSSCs are measured and compared. Fig. 4a presents the characteristic J–V curves for the DSSCs with different counter electrodes measured by AM1.5 illumination. For clarity, the derived photovoltaic parameters are summarized in Fig. 4b. Apparently, the best DSSCs performance ($J_{sc} = 12.56\ mA\ cm^{-2}$, $V_{oc} = 0.67\ V$, $FF = 0.71$ and $\eta = 5.93\%$) is obtained by using the nanograss-structured counter electrode with submicron-NG, which is better than that of the planar counter electrode ($J_{sc} = 11.21\ mA\ cm^{-2}$, $V_{oc} = 0.66\ V$, $FF = 0.69$ and $\eta = 5.15\%$). However, the efficiency of the cells with the nanograss length of 5 μm and 10 μm is much lower than that with planar counter electrode. The improvement of the efficiency η for the DSSCs with submicron-NG counter electrode in comparison with other counter electrodes can be attributed to the enhancement in the FF and the J_{sc}.

It is known that the FF and J_{sc} are determined by the total series resistance of the cell, which contains the sheet resistance of counter electrode, electron transport resistance, ion transport resistance, and the charge-transfer resistance at the interface of counter electrode [27]. For the DSSCs with the nanograss length of

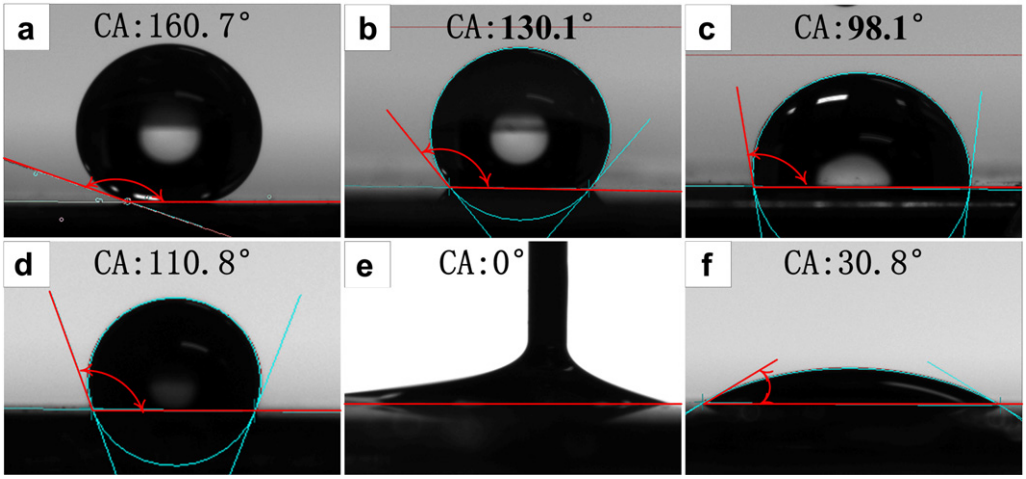

Fig. 3. The contact angle of water and electrolyte drops on various nanograss structure surfaces with bare and Pt layer coating, respectively. Water wetting on (a) bare silicon nanograss with the length about 5 μm, (b) 5 μm silicon nanograss sputtered with Pt, (c) planar silicon sputtered with Pt. And the contact angle of electrolyte wetting on (d) bare silicon nanograss with the length about 5 μm, (e) 5 μm silicon nanograss sputtered with Pt, (f) planar silicon sputtered with Pt.

5 μm and 10 μm, their efficiencies are much lower than that with planar counter electrode. The reason could be that, the aspect ratio of the silicon nanograss arrays was so high that it is difficult for Pt particles to reach the bottom of the nanograss by magnetic sputtering process. As shown in Fig. 2b, it clearly shows that the Pt layer were mainly coated on the top of the silicon nanograss, which leads to that the Pt layer is discontinuous and also not compact. In addition, the high aspect ratio of the silicon nanograss will result in a long electron collection distance. Therefore, the counter electrodes with such nanostructure will have a poor performance.

To further validate the good performance of submicron-NG counter electrode, the planar Pt/FTO/glass counter electrode based cells were also prepared in the same conditions. The corresponding photovoltaic characteristics ($V_{oc} = 0.67$ V, $J_{sc} = 10.88$ mA cm^{-2}, FF = 0.69, $\eta = 5.05\%$) are also shown in Fig. 4. The commonly used Pt/FTO/glass counter electrode exhibits slightly decreased energy-conversion efficiency in comparison with the planar silicon based counter electrode. A good counter electrode for DSSCs should have the characteristics such as good conductivity for transferring electrons or excellent catalytic activity for triiodide reduction or wonderful light scattering for improving light-harvesting efficiency [28]. In the following, we will explore the reason for the above DSSCs with such different performance, one section about the optics, and the others about the electrochemistry.

3.4. Reflection spectra of nanograss-structured counter electrode

The nanograss-structured counter electrode can enlarge the light pathway in diffuse reflection, not as the planar counter electrode in a specular reflection. So the Pt film in such structured DSSCs can more effectively reflect the unabsorbed light back to the photoanodes to improve the photon capture of solar cell. In this paper, the nanograss-structured counter electrode was measured by the diffuse reflection and specular reflection spectra, and the results were shown in Fig. 5. It demonstrates that the nanograss-structured counter electrodes have a good effect on light scattering. From the comparison of diffuse reflection (Fig. 5a) and specular reflection (Fig. 5b) spectra, we can infer the quantity of the reflection light deviating from the incident direction. In the Fig. 5a, planar counter electrode presents the strongest intensity of reflection, and submicron-NG, 5 μm and 10 μm NG counter electrodes show a lower reflection. The relatively low reflection of Pt/FTO/glass counter electrode may be due to the transmission of FTO glass, which is

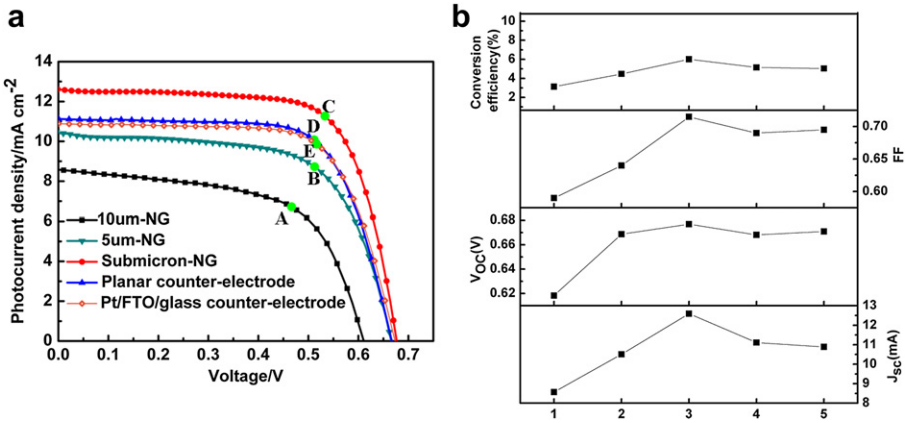

Fig. 4. (a) J–V curves of DSSCs based on the five different counter electrodes. A, B, C, D and E denote the point of the maximum power output. The maximum power corresponds visually to the area of the largest rectangle, which can fit inside the current–voltage curve. (b) Performance characteristics of DSSCs composed of five different counter electrodes. The irradiated area of the cells was kept at 0.25 cm^2. 1: the length of the nanograss for 10 μm, 2: the length of the nanograss for 5 μm, 3: Submicron counter electrode, 4: Planar counter electrode and 5: Pt/FTO/glass counter electrode.

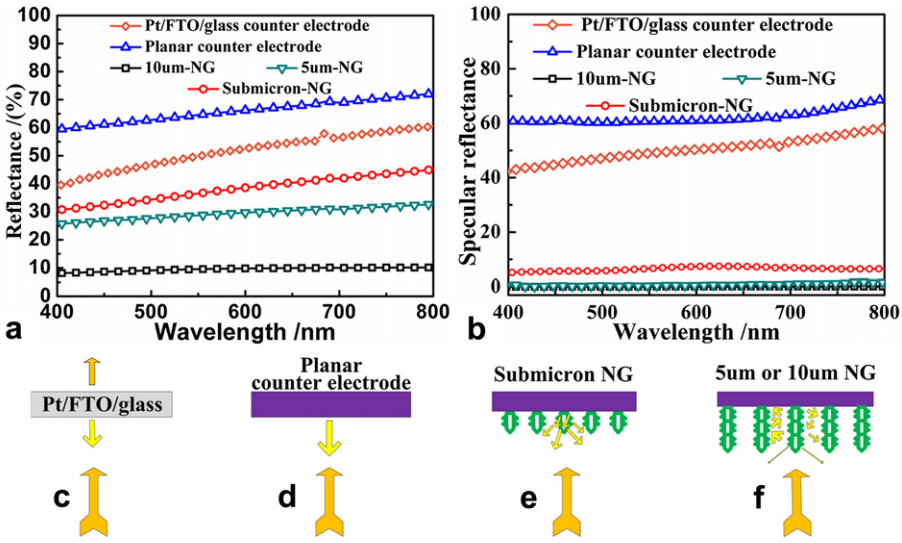

Fig. 5. (a) Diffuse reflection and (b) specular reflection spectra of various structured counter electrodes; schematic diagrams of (c) the incident light transmission through Pt/FTO/glass counter electrode, (d) specular reflection of planar silicon counter electrode, (e) light scattering of submicron-NG counter electrode and (f) light trapping of 5 μm or 10 μm NG counter electrode.

illustrated in the schematic diagram of Fig. 5c. Silicon substrate inherently possesses strong reflection, thus the reflection of the planar counter electrode based on silicon is enhanced and corresponding schematic diagram of Fig. 5d presents this case. The planar counter electrode based on silicon and conductive glass both show strong mirror-like reflection in Fig. 5b, indicating that all the reflected light may not be scattered away from the incident direction.

For the submicron-NG counter electrode, the specular reflection has a much larger decrease than the diffuse reflection, in comparison with planar Pt counter electrode based on silicon or glass. This comparison indicates that most of the light may be scattered away from the incident direction by the submicron-NG counter electrode. The difference in reflection of the planar and submicron-NG counter electrode may result from the strong light scattering on the structured surface of submicron-NG, which make light propagating in the active layer in multidirectional and oblique angles, thus increase the optical path length, the schematic diagram of Fig. 5e describes this case. For the 5 μm NG or 10 μm NG counter electrodes, the diffuse reflection and specular reflection are all very small, which indicates that most light may be depleted in the deep nanograss structure. The longer nanograss would limit the light into the counter electrode, thus the scattered light is difficult to return to the photo-anodes, and the schematic diagram of Fig. 5f illustrates this case.

The different light scattering effects of the nanograss-structured counter electrodes result from the light modulation of the nanograss structure. As the silicon nanograss structure has unique morphology and dimensions that close to the optical wavelengths. In addition, the nanograss has a backbone-like structure on lateral surface, which result in the light can easily be scattered and increase the optical pathway. As we know, some periodic gratings can diffract light into the solar cell, but only in some specific angles, the random nanograss structure can couple to incident light in a more broad range angles. Therefore, the silicon nanograss structure can more efficiently improve the light absorption. Usually, in order to increase the light absorption of the DSSCs, a light scattering layer of large particles is deposited on the TiO_2 film. In this paper, the NG structured counter electrode can offer a large surface area and light scattering effect synchronously. However, here the dimension of nanograss structure was not optimized, the light scattering effect of nanograss can be increased further by tuning the height, pitch and shape.

3.5. Effects of Si nanograss on charge-transfer resistance and electrolyte diffusion

The back transfer of injected electrons to the oxidized dye sensitizer and the recombination of electrons in the conduction band of TiO_2 with I_3^- ions diminish the photocurrent generation. To reduce or avoid current loss, transportation kinetics of I^- and I_3^- from and to the counter electrode should be fast enough.

EIS measurements are a frequently used technique to analyze the electrode reaction process and mechanisms involved [29]. In this work, EIS spectra technology was employed to compare the resistances existing in the counter electrode and the electrolyte. As shown in Fig. 6c for the schematic diagram, We assembled the

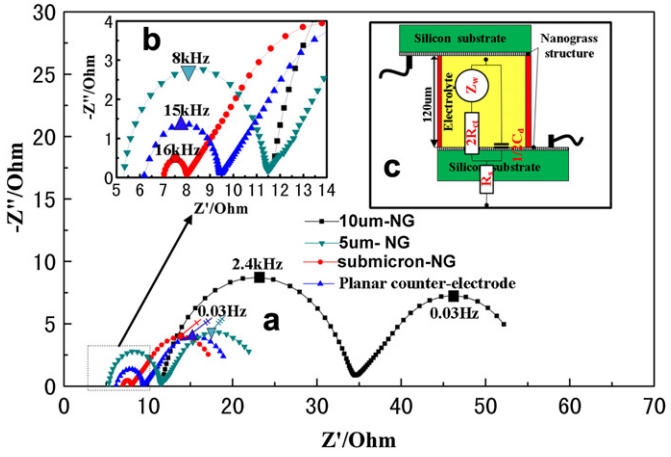

Fig. 6. (a) Typical Nyquist plots for four blank cells consisting of counter electrode|electrolyte|counter electrode with different structured electrodes in the dark under zero applied potential. The two semicircular shapes are assigned to impedances related to charge-transfer resistance at the Pt counter electrode in the high frequency region and ionic diffusion within the electrolyte in the low frequency region. (b) Inset represents the enlargement of the area for charge-transfer resistance of different types of counter electrodes, which is marked with rectangle of dotted lines (c) Electrochemical cell model used for EIS measurements and Equivalent circuit for the impedance spectrum of the blank cell. Z_w Nernst diffusion impedance of the electrolyte; R_{ct} charge-transfer resistance; C_d double-layer capacitance of one electrode; R_s: external serial ohmic resistance.

sandwiched blank cells with two identical counter electrodes to make the EIS measurement, and Fig. 6c also shows a representative equivalent circuit for this type of test assembly [8,16,30], where R_s is the ohmic serial resistance mainly related to the conductive substrates, R_{ct} is the charge-transfer resistance, C_d is the capacitance of electrical double-layer, and Z_w is the Nernst diffusion impedance of the electrolyte. The parameters R_{ct} and Z_w have been usually used to evaluate the influence of the counter electrode on the performance of the solar cells. In this literature, by fitting the plots with the equivalent circuit in Fig. 6c, we can acquire the R_s, R_{ct} and Z_w and to evaluate the influence of the electrode with ordered nanostructures on the performance of the DSSCs. Evidently, Fig. 6a exhibits typical Nyquist plots for the blank cells with various counter electrodes toward the I_3^-/I^- electrolyte, and we can clearly found that submicron-NG has the lowest total resistance. Furthermore, from the magnified image Fig. 6b, it is apparent that the submicron-NG has much lower R_{ct} values than the planar counter electrode, which suggests that structured counter electrodes have high electro-catalytic activities due to the high specific surface area. For the electrolyte diffusion, the above-mentioned wetting properties of nanograss structure validate that liquid electrolyte can penetrate into the nanograss structure more easily, which indicate that the nanograss structure may can improve the electrolyte diffusion. In our current experiment, the EIS measurement of the blank cells did not show the improved electrolyte diffusion evidently. Because the Warburg impedance of the electrolyte presented in the second semicircle of Fig. 6a is largely influenced by the gap between the two similar counter electrodes. The etched nanograss structure increases the gap, which may increase the impedance of the electrolyte diffusion [31,32]. The increased impedance will largely counterbalanced the favorable electrolyte penetration brought by the intrinsic properties of nanograss structure. However, the presented second semicircle for the planar, submicron and 5 μm NG have almost the same size, which indicates that the introduced nanograss structure can reduce the influence of increased gap to some extent and support the favorable electrolyte diffusion. Therefore, nanograss structure is suitable for smooth transfer of redox species in counter electrodes.

3.6. Electrochemical impedance spectra analysis of DSSCs

To further characterize the effects of the different counter electrodes on the photovoltaic properties, EIS measurements of the assembled DSSCs were performed in the illumination at open-circuit voltage conditions. The Nyquist plots of the cells are shown in Fig. 7, and the equivalent circuit is depicted in the inset [33]. In general, there are three semicircles in the Nyquist plot of DSSCs, and R_{S0} is the device's series resistance. The first semicircle at the high frequency range corresponds to the Pt/electrolyte interface, consisted of interfacial charge-transfer resistance (R_{CT1}) and constant phase element (CPE_1); The second semicircle at the middle frequency range is mainly attributed to the TiO_2/dye/electrolyte interface, consisted of interfacial charge-transfer resistance (R_{CT2}) and constant phase element (CPE_2); The third semicircle stems from the Warburg diffusion process of I^-/I_3^- in the electrolyte (Z_w) [34,35]. As shown in Fig. 7, the third semicircle of Z_w is not obvious because of the low viscosity of the present electrolyte and thinner spacer in our devices [36]. The corresponding fitted values of EIS measurements are listed in Table 1. Since the similar photo-anodes are used in the DSSCs, the characteristics of the counter electrodes are mainly responsible for the variation of EIS spectra. The R_{S0} of the DSSCs with planar, submicron-NG and 5 μm NG have a similar value, but the R_{S0} of 10 μm NG presents an obvious increase due to the discontinuous

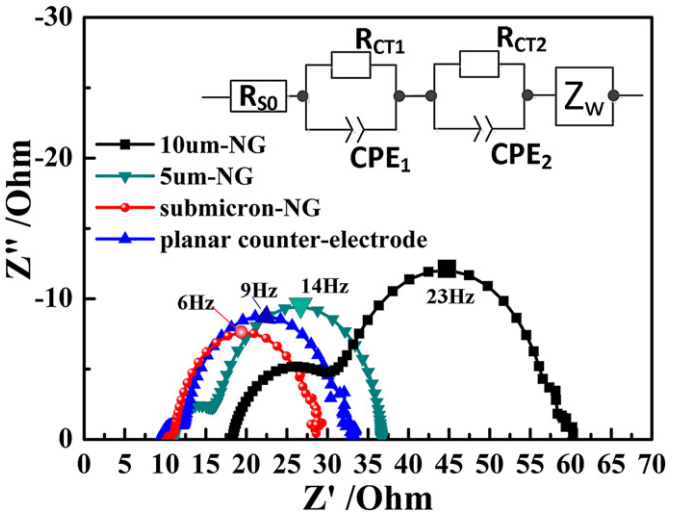

Fig. 7. Electrochemical impedance spectra of DSSCs based on different counter electrodes, measured at open-circuit voltage under an illumination intensity of 100 mW cm^{-2}. The inset shows the corresponding equivalent circuit used to fit the EIS spectra for DSSCs: R_{S0} is the series resistance; R_{CT1} and CPE_1 are the charge-transfer resistance and corresponding constant phase element at the counter electrode; R_{CT2} and CPE_2 represent the charge-transfer resistance and corresponding constant phase element at the TiO_2/dye/electrolyte interface; Z_W is the electrolyte diffusion resistance.

platinum film. The value of R_{CT1} is well in the same order with the EIS results of measured blank cells, and the submicron-NG counter electrode shows the smallest R_{CT1} among all the different counter electrodes based DSSCs. The decreased R_{CT1} and low R_{S0} could enhance the fill factors and energy-conversion efficiencies of the devices, which are also in consistency with the results of the J–V curves. Typically, the R_{CT2} should show a similar value for all measured DSSCs due to the only difference in counter electrodes. However, the increased light scattering from submicron-NG counter electrode means more dye excitation and more injected electrons to the conduction band of TiO_2, which cause a decrease in R_{CT2}. For the significant increased R_{CT2} of 10 μm-NG counter electrode based solar cell, it may be due to the weakened I^-/I_3^- circular reaction rate, increased distance between electrodes and serious light trapping, which result in less dye excitation and electron injection. Additionally, above observation of R_{CT2} is also in consistency with the corresponding value of J_{sc}. The change in energy-conversion efficiency is mainly related to the variation in the total resistance (R_{FULL}), which determines the photovoltaic performance of the DSSCs, because the Z_w is overlapped by R_{CT2}, so the R_{FULL} can be expressed as the sum of R_{S0}, R_{CT1} and R_{CT2} [33]. As shown in Table 1, the values of R_{FULL} increase in the order of submicron-NG, planar, 5 μm NG and 10 μm NG counter electrodes, the increased R_{FULL} results in the low fill factor and decreased conversion efficiency. The results of the EIS measurements are found to be in consistency with the results obtained from the photovoltaic characteristics, which further demonstrates that a structure-engineered counter electrode is one of the potential ways to improve the performance of DSSCs.

Table 1
Electrochemical impedance parameters of DSSCs based on various counter electrodes.

Counter electrodes	R_{S0}	R_{CT1} (ohm)	R_{CT2} (ohm)	$R_{S0}+R_{CT1}+R_{CT2}$ (ohm)
Planar counter electrode	9.93	2.63	19.33	31.89
Submicron-NG	10.01	0.48	17.37	27.86
5 μm NG	10.72	4.84	20.04	35.60
10 μm NG	18.92	14.83	25.30	59.05

4. Conclusion

In conclusion, the structured counter electrode for DSSCs had been investigated. A simple fabrication technique for silicon nanograss by means of dry etching process directly formed on Si substrates was proposed and demonstrated. A high energy-conversion efficiency of approximately 5.93% can be obtained for DSSCs based on a nanograss-structured counter electrode compared to a planar counter electrode 5.15%. The nanograss-structured counter electrode is important for exploring a new method to improve the performance of DSSCs by structuring the counter electrode. The results suggested that the orderly and sub-microstructure can have some effects and improvement on the performance of the DSSCs. However, the process needs further optimization of various parameters related with the etching processing conditions and metal deposition, which may result in further improvement in cell performance. Therefore, in order to acquire a preferred performance, exploring how to structure the counter electrodes, such as grating, pillars, and porous structures and so on, is also a much better choice.

Acknowledgment

This work is supported by National Natural Science Foundation of China (No. 90923040, 50975226), National Science and Technology Project (No. 2011ZX04014-071), National Basic Research Program of China (No. 2009CB724202), and the Fundamental Research Funds for the Central Universities.

References

[1] A. Yella, H.W. Lee, H.N. Tsao, C.Y. Yi, A.K. Chandiran, M.K. Nazeeruddin, E.W.G. Diau, C.Y. Yeh, S.M. Zakeeruddin, M. Gratzel, Science 334 (2011) 629–634.
[2] B. Oregan, M. Gratzel, Nature 353 (1991) 737–740.
[3] X.Z. Zhao, C.H. Zhou, Y. Yang, J. Zhang, S. Xu, S.J. Wu, H. Hu, B.L. Chen, Q.D. Tai, Z.H. Sun, Electrochimica Acta 54 (2009) 5320–5325.
[4] A. Kay, M. Gratzel, Solar Energy Materials and Solar Cells 44 (1996) 99–117.
[5] B. Fang, M. Kim, S.-Q. Fan, J.H. Kim, D.P. Wilkinson, J. Ko, J.-S. Yu, Journal of Materials Chemistry 21 (2011) 8742–8748.
[6] H. Choi, H. Kim, S. Hwang, W. Choi, M. Jeon, Solar Energy Materials and Solar Cells 95 (2011) 323–325.
[7] K. Suzuki, M. Yamaguchi, M. Kumagai, S. Yanagida, Chemistry Letters 32 (2003) 28–29.
[8] J.D. Roy-Mayhew, D.J. Bozym, C. Punckt, I.A. Aksay, ACS Nano 4 (2010) 6203–6211.
[9] J. Xia, L. Chen, S. Yanagida, Journal of Materials Chemistry 21 (2011) 4644–4649.
[10] Y. Yoshida, S. Yamaguchi, K. Maeda, Analytical Sciences 26 (2010) 137–139.
[11] T.N. Murakami, M. Grätzel, Inorganica Chimica Acta 361 (2008) 572–580.
[12] X. Yin, Z. Xue, B. Liu, Journal of Power Sources 196 (2011) 2422–2426.
[13] J.S. Jang, D.J. Ham, E. Ramasamy, J. Lee, J.S. Lee, Chemical Communications 46 (2010) 8600–8602.
[14] W. Vallejo, C. Quinones, F. Mesa, Applied Surface Science 257 (2011) 7545–7550.
[15] N. Papageorgiou, Coordination Chemistry Review 248 (2004) 1421–1446.
[16] A. Hauch, A. Georg, Electrochimica Acta 46 (2001) 3457–3466.
[17] G. Khelashvili, S. Behrens, C. Weidenthaler, C. Vetter, A. Hinsch, R. Kern, K. Skupien, E. Dinjus, H. Bonnemann, Thin Solid Films 511 (2006) 342–348.
[18] W.B. Wang, Z. Luo, X.R. Xiao, Y. Lin, Chinese Journal of Chemistry 22 (2004) 256–258.
[19] R.T.R. Kumar, K.B. Mogensen, P. Boggild, Journal of Physical Chemistry C 114 (2010) 2936–2940.
[20] J. Shieh, F.J. Hou, Y.C. Chen, H.M. Chen, S.P. Yang, C.C. Cheng, H.L. Chen, Advanced Materials 22 (2010) 597.
[21] M. Mehran, S. Mohajerzadeh, Z. Sanaee, Y. Abdi, Applied Physics Letters 96 (2010).
[22] J. Shieh, C.H. Lin, M.C. Yang, Journal of Physics D Applied Physics 40 (2007) 2242–2246.
[23] H. Sai, H. Fujii, K. Arafune, Y. Ohshita, M. Yamaguchi, Y. Kanamori, H. Yugami, Applied Physics Letters 88 (2006).
[24] A.Y. Vorobyev, C.L. Guo, Applied Surface Science 257 (2011) 7291–7294.
[25] M. Otto, M. Kroll, T. Kasebier, S.M. Lee, M. Putkonen, R. Salzer, P.T. Miclea, R.B. Wehrspohn, Advanced Materials 22 (2010) 5035.
[26] J.H. Oh, T.G. Deutsch, H.C. Yuan, H.M. Branz, Energy & Environmental Science 4 (2011) 1690–1694.
[27] M. Wang, P. Chen, R. Humphry-Baker, S.M. Zakeeruddin, M. Grätzel, Chemphyschem 10 (2009) 290–299.
[28] F. Fabregat-Santiago, G. Garcia-Belmonte, I. Mora-Sero, J. Bisquert, Physical Chemistry Chemical Physics 13 (2011) 9083–9118.
[29] N. Papageorgiou, W.F. Maier, M. Gratzel, Journal of Electrochemical Society 144 (1997) 876–884.
[30] G. Wang, W. Xing, S. Zhuo, Journal of Power Sources 194 (2009) 568–573.
[31] T. Hoshikawa, M. Yamada, R. Kikuchi, K. Eguchi, Journal of Electrochemical Society 152 (2005) E68–E73.
[32] R. Kern, R. Sastrawan, J. Ferber, R. Stangl, J. Luther, Electrochimica Acta 47 (2002) 4213–4225.
[33] L. Han, N. Koide, Y. Chiba, A. Islam, R. Komiya, N. Fuke, A. Fukui, R. Yamanaka, Applied Physics Letters 86 (2005) 213501–213503.
[34] M. Itagaki, K. Hoshino, Y. Nakano, I. Shitanda, K. Watanabe, Journal of Power Sources 195 (2010) 6905–6923.
[35] F. Fabregat-Santiago, J. Bisquert, E. Palomares, L. Otero, D. Kuang, S.M. Zakeeruddin, M. Grätzel, Journal of Physical Chemistry C 111 (2007) 6550–6560.
[36] L.-Y. Lin, C.-P. Lee, R. .Vittal, K.-C. Ho, Journal of Power Sources 196 (2011) 1671–1676.